DEVELOPMENT AND VALIDATION OF MODELS FOR DURABILITY ESTIMATION OF EXHAUST MANIFOLDS UNDER HIGH TEMPERATURES

M. Wendt*, W. Rehm**

*) Daimler AG, Mercedes-Benz Werk Hamburg, 21160 Hamburg, Germany

**) Daimler AG, Forschung und Vorentwicklung, 89081 Ulm, Germany

ABSTRACT

Air-gap insulated exhaust manifolds are mainly stressed by thermo-mechanical loads (TMF). To calculate the components with regard to their durability, a material model was created using a nonlinear kinematic model of strain hardening based on Low-Cycle-Fatique-(LCF)-tests and multi-level creep tests. On this basis, an energy-based model for life estimation was developed. The simulation of the LCF tests showed a good correlation. The model was validated on the hot gas test rig using a bended pipe. Furthermore, a model was developed to calculate welds. LCF tests with welded specimens were carried out and based on these tests, the material model of the basic material was modified for the welded areas.

KEYWORDS

Exhaust manifolds, thermo-mechanical loads, strain hardening, life estimation model, welded joints

INTRODUCTION

The LSI exhaust manifolds used by Mercedes are released on the basis of tests. However, in order to save development times, the demands on the Finite Element Simulation are becoming ever higher. In order to make reliable statements about the durability, material and life models for the materials used were developed. This is described in this contribution.

The article is an extended version of the paper submitted for the proceedings of the “Fourth International Conference on Material and Component Performance under Variable Amplitude Loading (VAL4)” which was scheduled for May/April 2020 and unfortunately cancelled because of the Covid 19-virus, [1].

1. DESIGN OF LSI EXHAUST MANIFOLD

Double-walled exhaust manifolds are used in vehicles of the Mercedes brand as well as single-walled cast exhaust manifolds. Compared to cast manifolds, double-walled manifolds are less hot on the outer surface and less subject to relative movements to connected parts. Double-walled manifolds consist of inner tubes and an outer shell. The inner tubes take over the gas supply, the protective shell seals to the outside, Fig. 1. Between the tubes and the shell lies an air cushion, which insulates thermally. This manifold design is also referred to as an LSI (Air-Gap-Insulated) exhaust manifold.

The Insulation is the reason why the temperatures on the outside are lower than on the cast manifold. This allows more flexibility for the design of other vehicle components in the vicinity of the manifold. Here, less heat resistant materials may be used and distances to the manifold may be smaller. This reduces costs and saves space in the engine compartment. On the other hand, the gas keeps hot until it reaches the turbocharger and catalytic converter, especially when the motor is cold. This improves the efficiency of both, the charger and the converter.

The gas guide is not tight: it consists of several pieces of pipe which are stuck into each other, Fig. 1 (right). In these overlap areas, the pipe pieces can move relatively to each other. This allows a free thermal expansion of the material. Without the possibility of free expansion, the inner tubes, which become very hot, would be subject to great stresses. But the freedom to move relatively to each other in the longitudinal direction prevents overloads. The parts that make up the protective shell, Fig. 1 (left) are not movable relatively to each other. Because the shell is on the outside, it is less hot and therefore less subject to thermal expansion. Thus, the resulting thermo-mechanical stresses remain low enough.

Another effect of the lower thermal expansion is that the elastic and plastic deformations of the manifold relative to supports are lower. In particular, the motion and deformation of the manifold flanges relative to the cylinder head in longitudinal and in normal direction could cause failure of the gasket to the cylinder head. Elastic and plastic deformations in normal direction are caused by bending of the manifold when inhomogeneous temperature fields are applied. Compared to single-walled cast manifolds, double-walled manifolds like the described LSI manifolds show less relative motion to the cylinder head as the load-bearing structure becomes less hot.

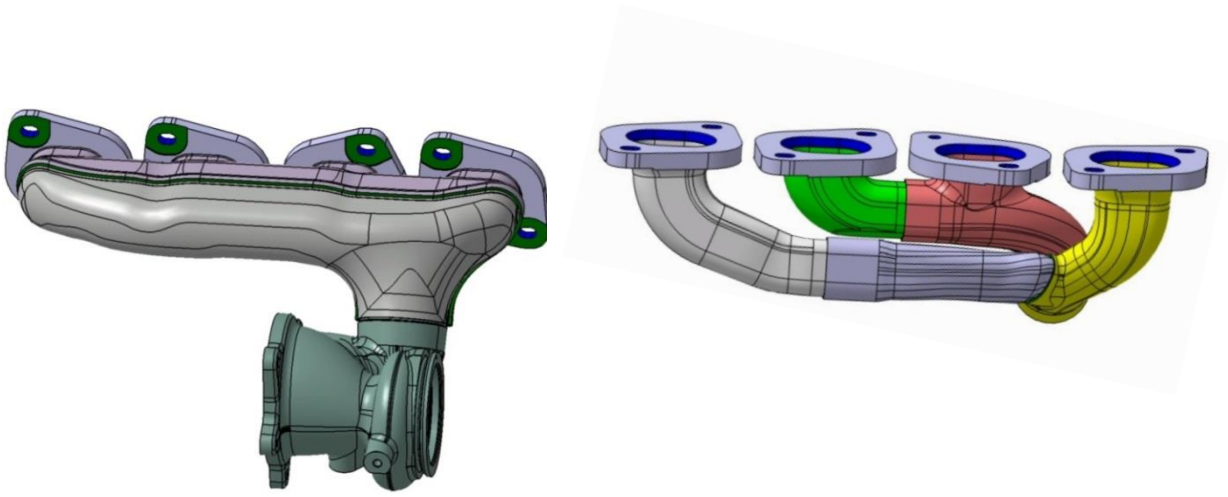

Fig. 1: Design of LSI exhaust manifold. Left: Seen from the outside (outer shell with flanges and turbocharger housing). Right: Inner Parts with flanges.

Both, the gas guide and the protective shell are made of high-alloy, high-temperature resistant sheet metal materials, usually austenitic stainless steels, such as X5CrNi18 or higher alloyed, see Table 1. The materials are connected using MAG or WIG welding processes.

	C	Si	Mn	P	S	Cr	Ni	N
min.	-	-	-	-	-	17,5	8	-
max.	0,07	1	2	0,045	0,03	19,5	10,5	0,1

HB Hardness	E [Gpa] Modulus of Elasticity	Rp0,2 [Mpa] 0.2%-Yield Strength	Rm [Mpa] Tensile Strength	As [%] Elongation
< 215	200	> 190	> 500	> 45

Table 1: Chemical composition and mechanical Properties of X5CrNi18.

The protective shell consists of two deep-drawn parts welded together. The pipe sections of the gas guide are made of sheet metal tubes in the hydroforming (IHU) process. The hydroformed pipe sections are welded together with the protective shell to the flanges. There is another weld for the connection to the turbocharger housing. There are also exhaust manifolds where the turbocharger is clamped to an extra flange of the manifold.

The LSI exhaust manifolds are manufactured at the Daimler plant in Hamburg. The development of the manifolds is also carried out in Hamburg, in cooperation with Stuttgart development departments. The research and pre-development department Ulm supported basic research. The investigations described in this article were done in cooperation of the three areas in Hamburg, Stuttgart and Ulm.

2. LOADS ON EXHAUST MANIFOLDS

The exhaust manifold is subject to mechanical and thermal loads, Fig. 2a. On the manifold exhaust gas streams act with temperatures up to 1000 ° C. Since the manifold is generally not cooled actively, it is the hottest component of the entire vehicle.

The pure thermal load can lead to corrosion and lack of rigidity of the manifold. More critical, however, is the thermo-mechanical stress created by the temperature: The thermal expansion causes the components to become distorted so that they can fail. Furthermore, the materials are subject to strong creep at high temperatures.

The load is variable: By heating and cooling the engine and the manifold, the manifold is subject to fatigue loading. However, since only a relatively small number of hot-cold load changes occur in motor life, the loading is referred to as low-cycle fatique loading (LCF) in opposite to high-cycle fatique loading (HCF), which is tested using classic methods of fatigue life. In addition to the LCF load, HCF loads due to vibrations are also present at the manifold, the loads are superimposed.

Exhaust manifolds are tested on motor test rigs where different load courses with variable loads are applied, see example in Fig. 2d. Other tests are carried out using 2-point-load-cycles, Fig. 2b. While the temperature of the exhaust gas is reached nearly instantly, the temperature at different points on the manifold lags behind and builds up differently at different points. Stresses and strains at certain points have completely different time history courses, depending on the position on the manifold. At some positions, the stress even increases while the temperature decreases, Fig. 2c. Thus, the amplitudes as well as the curve characteristics vary depending on the location. In FE-calculations at least three cycles are simulated as the amplitudes vary during the first cycles until the system has settled.

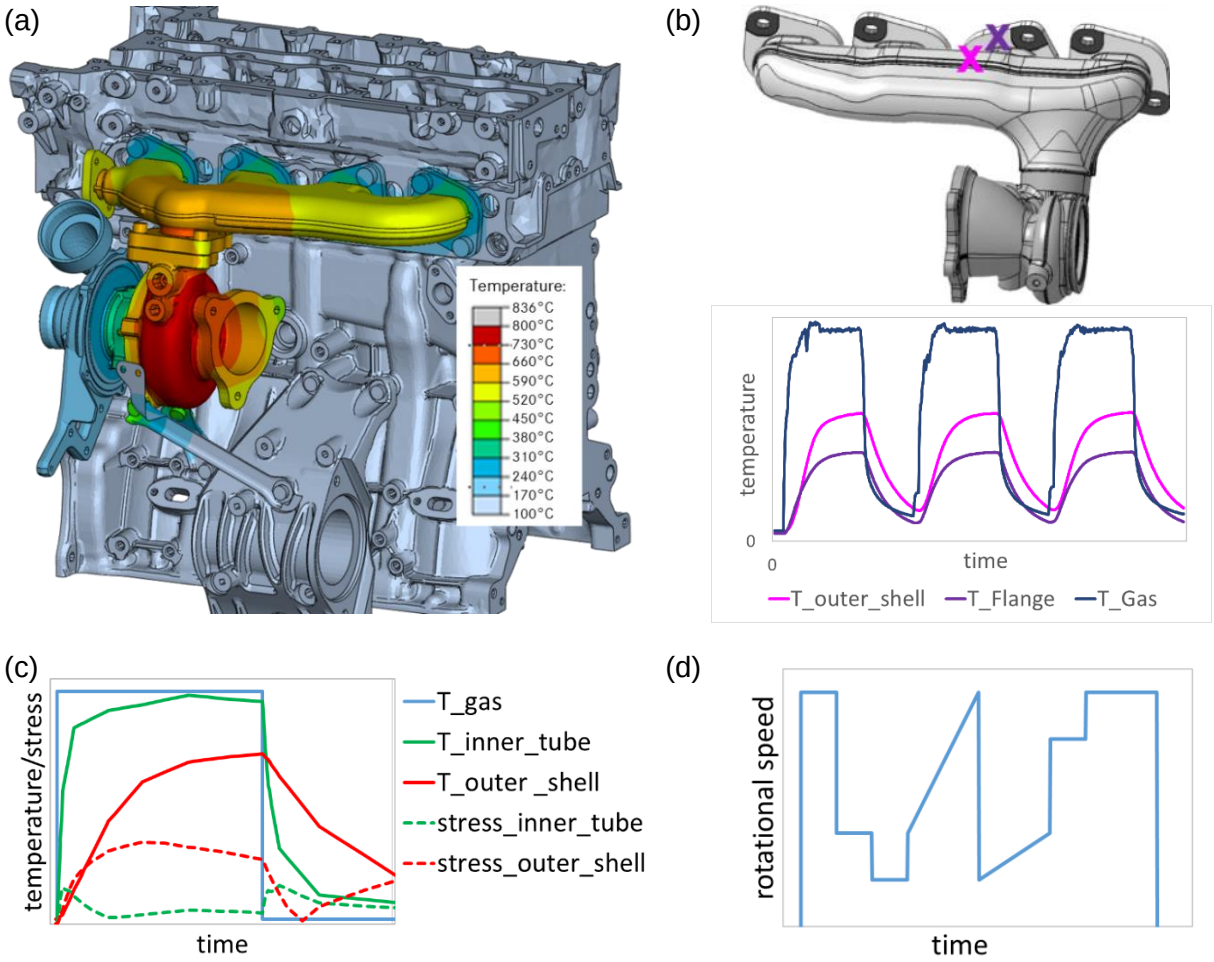

Fig. 2: (a) Temperature field of exhaust manifold. Colored representation of temperatures on manifold and turbocharger housing, (b) course of gas temperature as well as temperatures at the points marked on the manifold, measured on a hot gas test rig, (c) course of temperatures as well as stresses at certain points of the manifold, (d) qualitative course of rotational speed on a motor test rig (example).

3. MODELING OF SHEET METAL MATERIAL

Material Behaviour under Cyclic Loads

In general, the flow behavior in non-linear FEM programs is calculated with the following procedure: the increase of stress at given strain runs along the yield curve after reaching the yield point, area (1) in Fig. 3a.

While unloading, the stress runs linear in the stress-strain diagram. That means, the hardening experienced by the material leads to a new, higher yield strength. When reloading, the material is then plasticized only after reaching the first maximum stress (new yield strength). This model is well suited to account for strain hardening as long as stress remains in the first quadrant of the stress-strain diagram.

For alternating loads, e.g. tension and compression, the model leads to unrealistic behavior, as shown in in Fig. 3a: At first loading up to ε_0 (e.g. tension), the yield strength is shifted the

first time, area (1). At the second loading (e.g. pressure), the material in the negative region is plasticized a lot more, because of the shifted yield stress, area (2). At loading up to $-\varepsilon_0$, the material is then further hardened and the yield strength has risen. This increase occurs in each cycle, so that the yield strength continues to increase and the yield area becomes larger and larger. This model is called the isotropic hardening model, because the yield points are the same in all directions and the yield area is symmetrical to the origin. The progressive rising behaviour with changing load, however, does not correspond to reality. Therefore, a nonlinear kinematic hardening model is used to describe the material behavior of the exhaust manifold.

In the kinematic hardening model, the yield area is displaced in the corresponding direction under load and not expanded, in Fig. 3b. This results in plasticization much earlier if the load is reversed, range (2). The yield strength is not increased (point **), but on the contrary, it is reached much earlier. When re-loaded in the opposite direction, the plasticization also starts early, so that sets no progressive rising occurs and a stable hysteresis curve results quickly in under repeatedly changing loads. The yield area is displaced every cycle. This allows to model a realistic material behavior, even for cyclic loads.

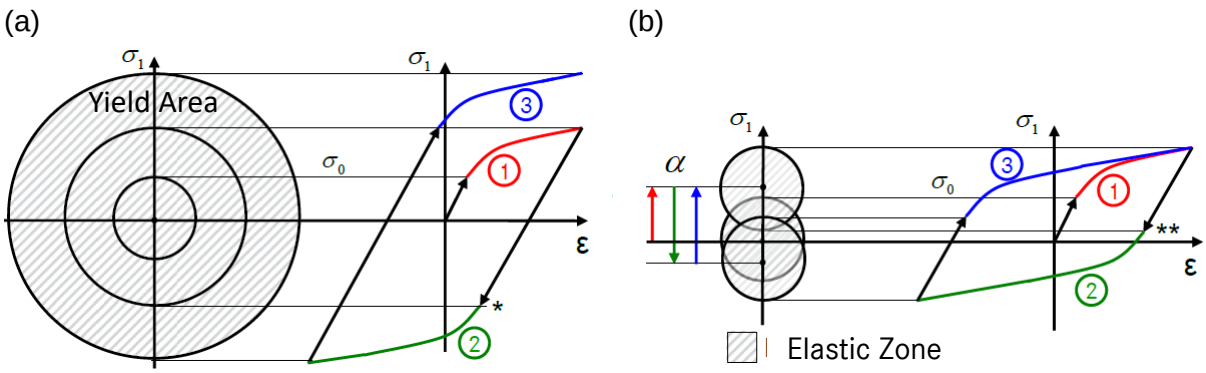

Fig. 3: (a) Isotropic hardening model and (b) kinematic hardening model.

Mathematically, the behavior is described by several differential equations for the so-called backstresses α_k,

$$\sigma = \sigma_0 + \sum \alpha_k \quad , \quad \dot{\alpha}_k = C_k \cdot \frac{1}{\sigma_0} \cdot (\sigma - \alpha) \cdot \dot{\varepsilon}_{pl} - \gamma_k \cdot \alpha_k \cdot \dot{\varepsilon}_{pl} \quad .$$

The backstresses α_k indicate how far the yield area is displaced. This model is implemented in the FEM program ABAQUS. In order to use the model, the coefficients C_k and γ_k must first be determined by fitting to measured hysteresis curves.

Tests

In order to adapt the nonlinear kinematic material model, a series of LCF experiments were carried out. That were experiments in which a tensile specimen is loaded alternately, the strain amplitude being so high that the specimen cracks with less than 10,000 load cycles. The temperature was kept constant during one experiment.

Tubes as shown in Fig. 4 were used as test specimens. They were tested under tensile and compressive loads. From the sheets used in the manifold no suitable test specimens could be produced because flat tensile specimens would buckle under pressure load. Therefore, tubes with the same material properties were used. They cannot buckle under pressure and in contrast to solid material they have a similar hardening grade as sheet metals.

The specimens were inductively heated and pulsed, Fig. 4. There were experiments at 6 temperature levels and 3 strain amplitudes per temperature step. Stress ratio was R = -1. In addition, as an example, some experiments were carried out at R = -3 and R = 1/3 and experiments with different strain rates in order to determine the quality of the approximation for it. In addition, there were several TMF experiments in which the temperature was changed during cyclic loading.

In order to be able to map the creep behavior, step creep tests were carried out, also at 6 temperature levels. There were 12 strain levels per temperature, each temperature was kept for 30 minutes.

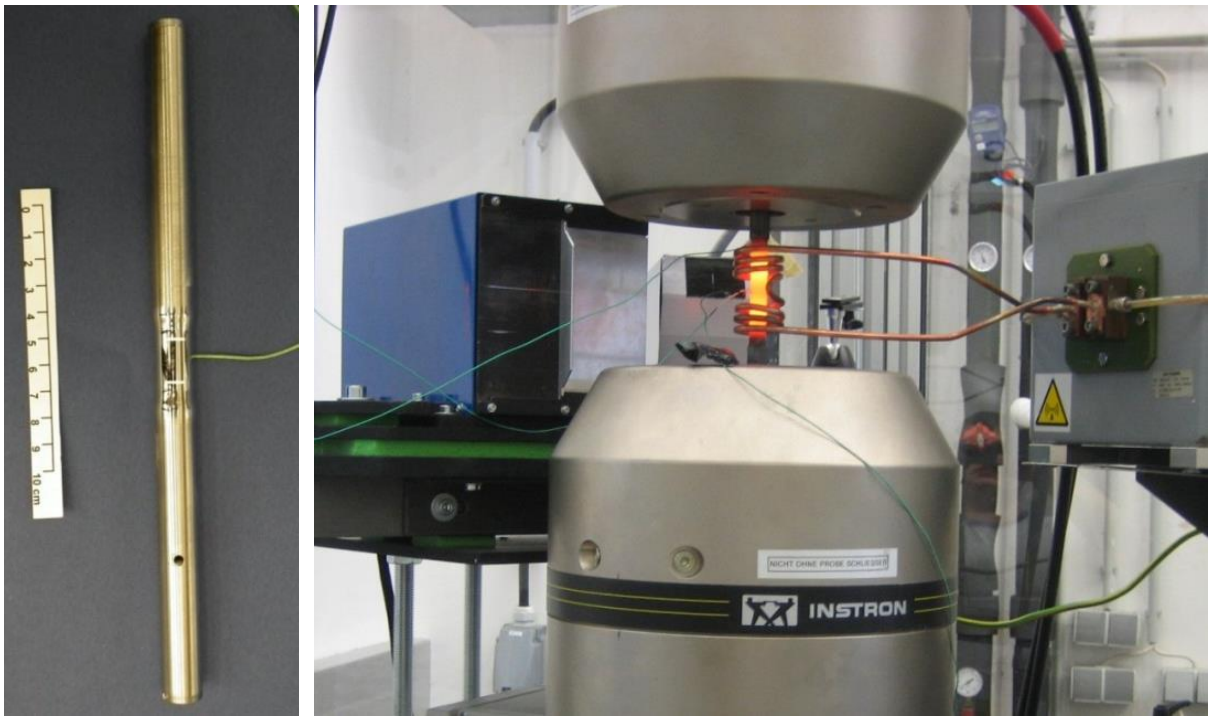

Fig. 4: Specimen and experimental setup for LCF and step creep tests.

Determination of Model Parameters

All measured hysteresis curves were recalculated using a Finite Element model. The model parameters C_k and γ_k were optimized so that the best possible approximation was found for all 17 T-ε-combinations. The result of the approximation is shown by an example in Fig. 5a.

Based on the creep tests, Fig. 5b, the creep law was determined. For this purpose, the exponential approach proposed in ABAQUS (strain hardening) was used,

$$\dot{\bar{\varepsilon}}^{cr} = (\mathrm{A}\tilde{q}^{n}[(m+1)\,\bar{\varepsilon}^{cr}]^{m})^{\frac{1}{m+1}}$$

.

The parameters *A, n,* and *m* were determined for each temperature level. The result of the fitting is very good, as seen in Fig. 5b. Within the FEM, the creep strains can be superposed with plastic and elastic strains.

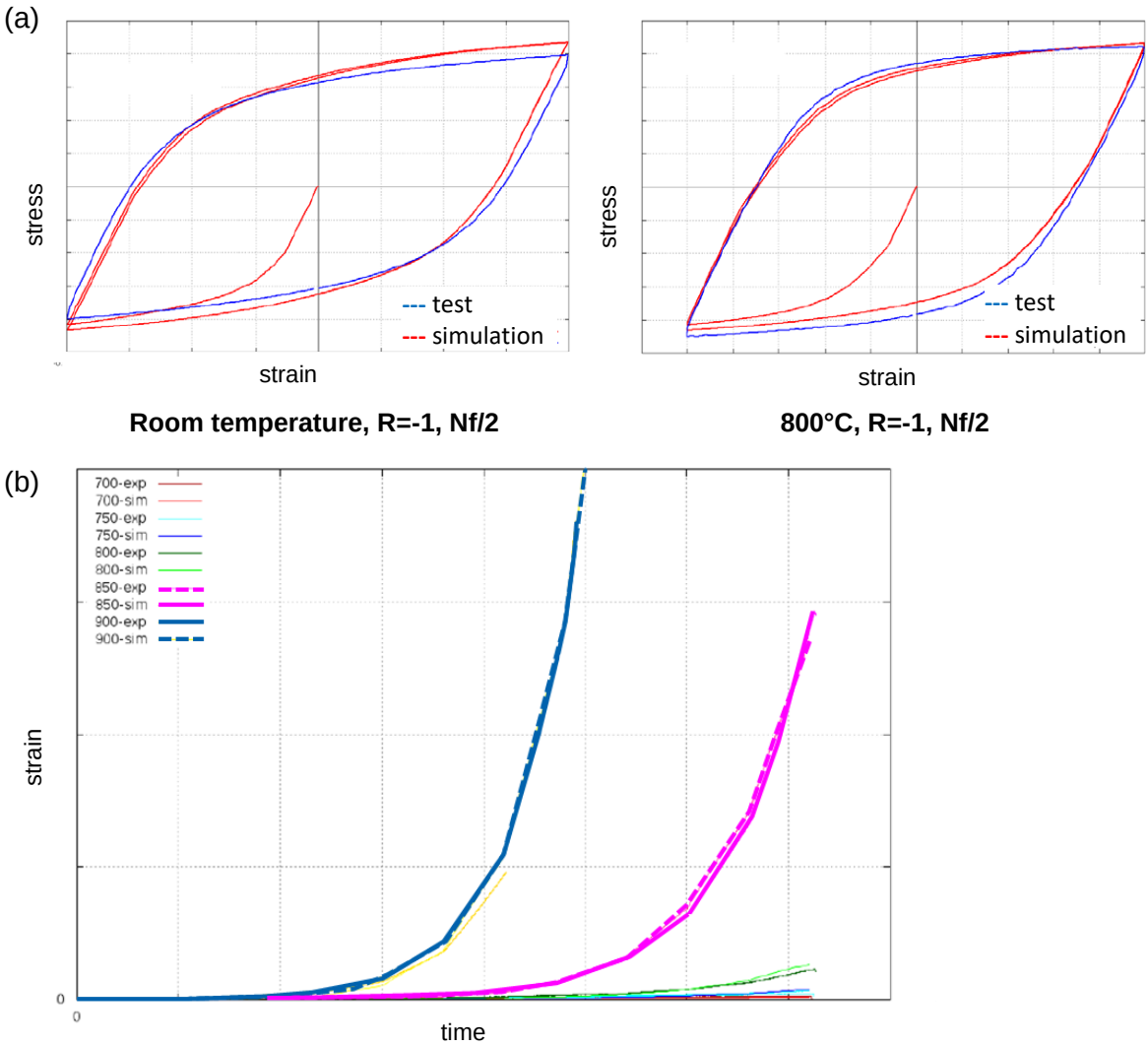

Fig. 5: (a) Comparison test and simulation, example of 2 LCF experiments. The curves were optimized for NF/2, this means for half cracking lifetime, (b) test and simulation of creep strains during the step creep test.

Life Estimation Model

On the basis of the LCF experiments not only the material model was adapted, but also a lifetime model was created. The damage parameter used is not stress or strain, as it is typical in Wöhler analyzes, but an energy-based damage parameter. The plastification energy and the creep energy are included in the calculation of the parameter. Between the damage parameter and the lifetime *Nf* of the specimens in the LCF experiment, a logarithmic relationship could be found,

$$Nf = p*D - q.$$

The parameters *p* and *q* were be determined for the 50% line. There is a good correlation between damage parameter and lifetime, Fig. 6a. Thus, the life of components can be predicted well. Also the comparison of the calculated lifetime with the experimental lifetime shows a good correlation, Fig. 6b. The regression lines show that almost all results are within the tolerance range of factor 2. In the horizontal direction (tolerance of lifetime) in Fig. 6a , this corresponds to a factor of 3.

a)

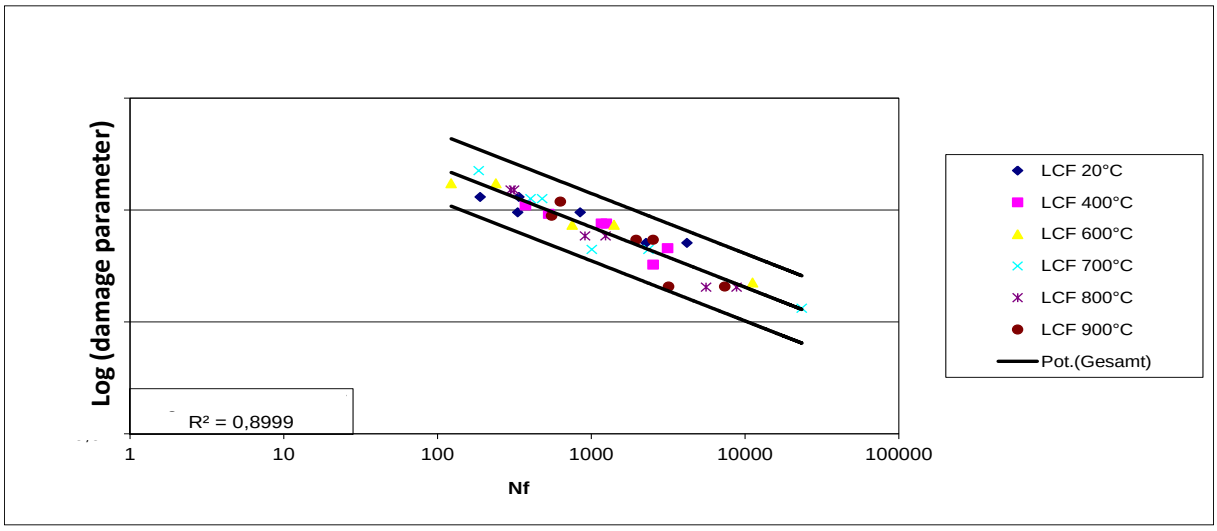

b)

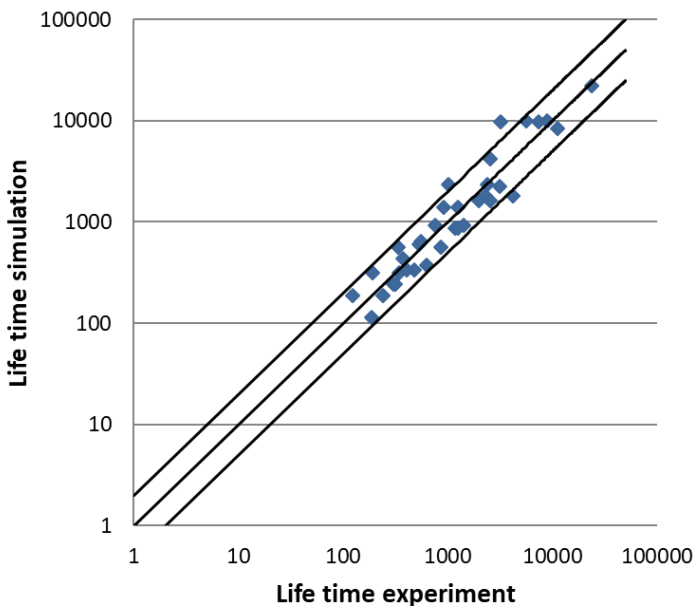

Fig. 6: (a) Lifetime model based on energy, (b) correlation between test and simulation.

4. VALIDATION

The illustrated correlation between experiment and calculation refers to the recalculated LCF experiments. In order to be able to check how good the lifetime calculation is for a real component, a validation test was set up. However, no exhaust manifold was tested, because then the cracks could also occur in the welds. Instead, a test specimen made from the same tube as the inner tubes of the manifold was used. In order to generate thermo-mechanical stresses, the tube was bent several times and afterwards firmly clamped on the hot gas test rig at both ends, Fig. 7a. Then, hot and cold gas alternately flowed through the specimen.

The aim of the validation test was the generation of cracks in the base material with fewer than 1500 load cycles and the verification of the result by a lifetime calculation.

Results Test on Hot Gas Test Rig

The first test was run for up to 1109 cycles, after which the test specimen was examined. It showed a visible crack at the side in the curved area, which could also be detected by endoscopy and bladder test, Fig. 7b.

A problem in the evaluation of the experiment is the determination of cracks during the run of the experiment. Not all cracks can be seen from the outside, as they can also start from the inside. Therefore, the tube was examined at intervals (after 475 and 747 cycles) by endoscopy: it was without findings. However, proof of a crack can only be obtained by destructive testing.

In the second test, a back pressure flap was welded to the end of the tube to increase the gas pressure. The test was run for up to 1380 cycles and stopped without visible cracks. The endoscopy was without findings after 331 cycles and also at the end of the test. Thereafter, the tube was destructively examined. By means of dye penetration examination, crack initiation could be detected on the inside in the same area as in experiment no. 1, Fig. 7c. This shows the difficulty of the evaluation: Since the endoscopy was without findings at the end of the experiment, it cannot be used as a meaningful method. It can only be speculated, at which number of load cycles the crack had emerged.

Results of Finite Element Calculation

The experiment was recalculated using the FEM with the same load profile. 30 cycles were calculated to cover transient phenomena completely. The energy values of the last cycle were transferred to the lifetime model and thus the initial cracking lives Nf were calculated, Fig. 8. According to the calculation, 335 load changes can be applied up to the start of a crack on the inside and 884 cycles up to the start of a crack on the outside. Crack growth is not calculated.

Assessment of the validation test

335 load changes until start of a crack in the calculation have to be compared with a proven complete crack with a load change number $Nf \leq 1109$ and the start of a crack with $Nf \leq 1390$ in the experiments. The evaluation must take into account that the reliable prediction of the crack life in the LCF experiments had a factor of 3, meaning that the start of a crack between 112 and 1005 load cycles is likely. Furthermore, it must be taken into account that the calculation only predicts the crack initiation, but the initiation cannot be clearly determined in the experiment. Thus, the prediction accuracy is within the usual accuracy in lifetime calculations. This must be taken into account when using the model.

An even more accurate prediction of lifetimes, in particular a prediction of crack growth to breakthrough would be desirable, but this is not possible under realistic conditions. However, another attempt was planned to provoke crack initiation on the outside to better determine when the crack begins.

(a)

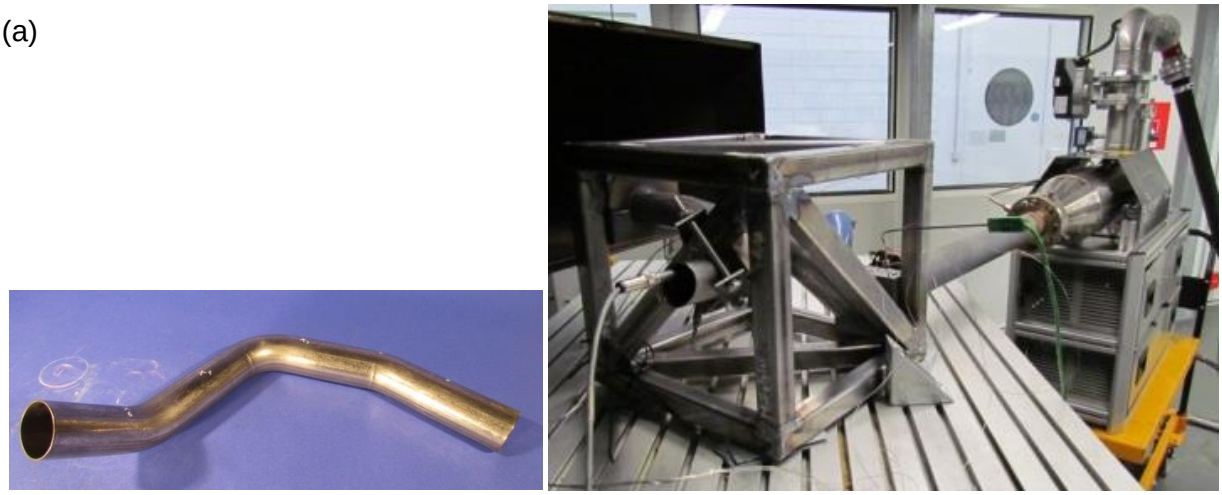

(b)

(c)

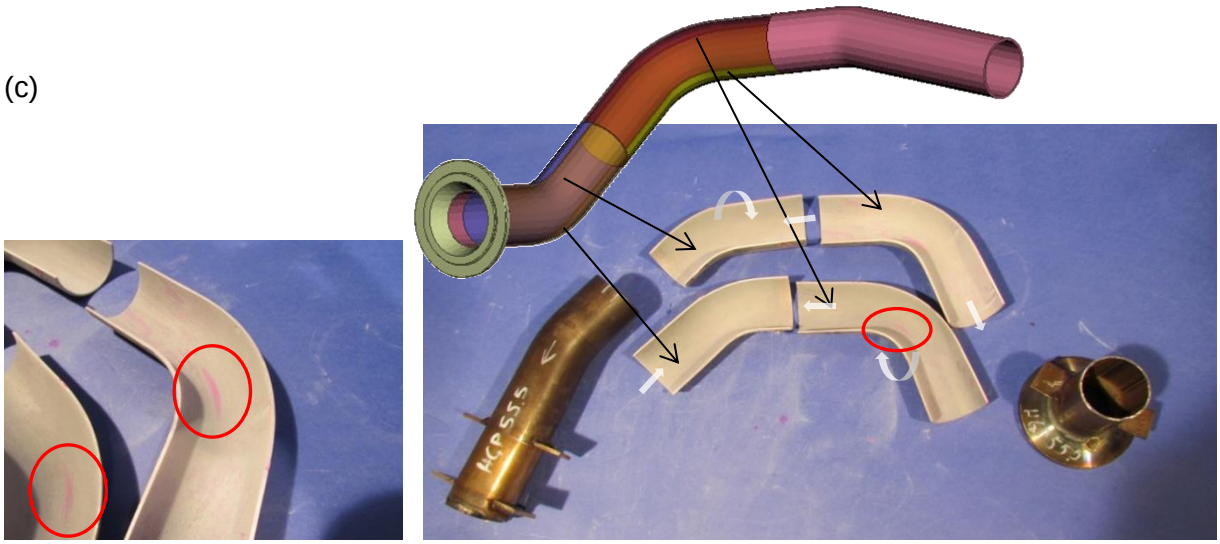

Fig. 7: (a) Test specimen (left) and setup of the validation test on the hot gas test bench (right), (b) test specimen from experiment 1 after 1109 cycles: Crack visible on the side of the arch (left). Detectable also by endoscopy (middle) and bladder test (right), (c) test specimen of experiment 2 after 1380 cycles. Color penetration test: elephant skin on the outside, crack initiation on the inside in the bow.

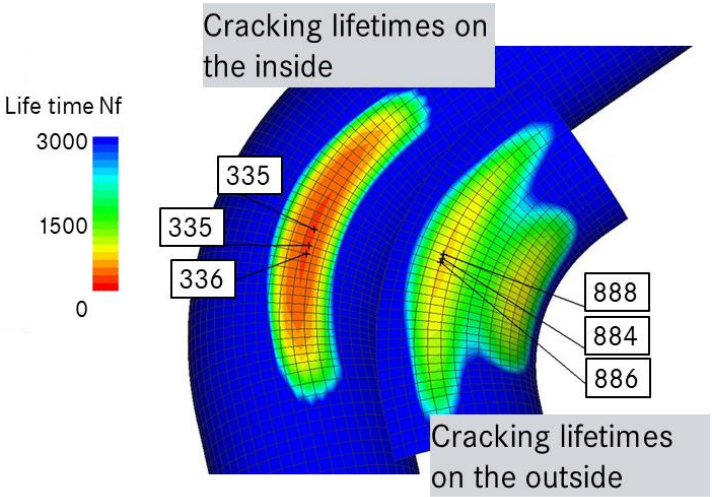

Fig. 8: Result of life calculation based on FEM. Left: Cracking lifetimes on the inside, right above: Cracking lifetimes on the outside of the tube.

5. APPLICATION IN LIFE ESTIMATION OF EXHAUST MANIFOLDS

The models described are currently were tested in the manifold calculation. It was examined how good the statements were in relation to the usual evaluation of the increase in plastic strain. Some of the hotspots are rated differently than before by the new process. In the example shown in Fig. 9, when evaluating the strain, a critical position on the protective tube of 2.6% plastic strain (PEEQ) was assessed to be significantly stronger than the second critical position (0.6%). When evaluating the lifetimes, the difference between these two positions is much lower (2141 load changes, as opposed to 3015 load cycles). One possible reason is that not only the plastification energy but also the creep energy is included in the lifetime model.

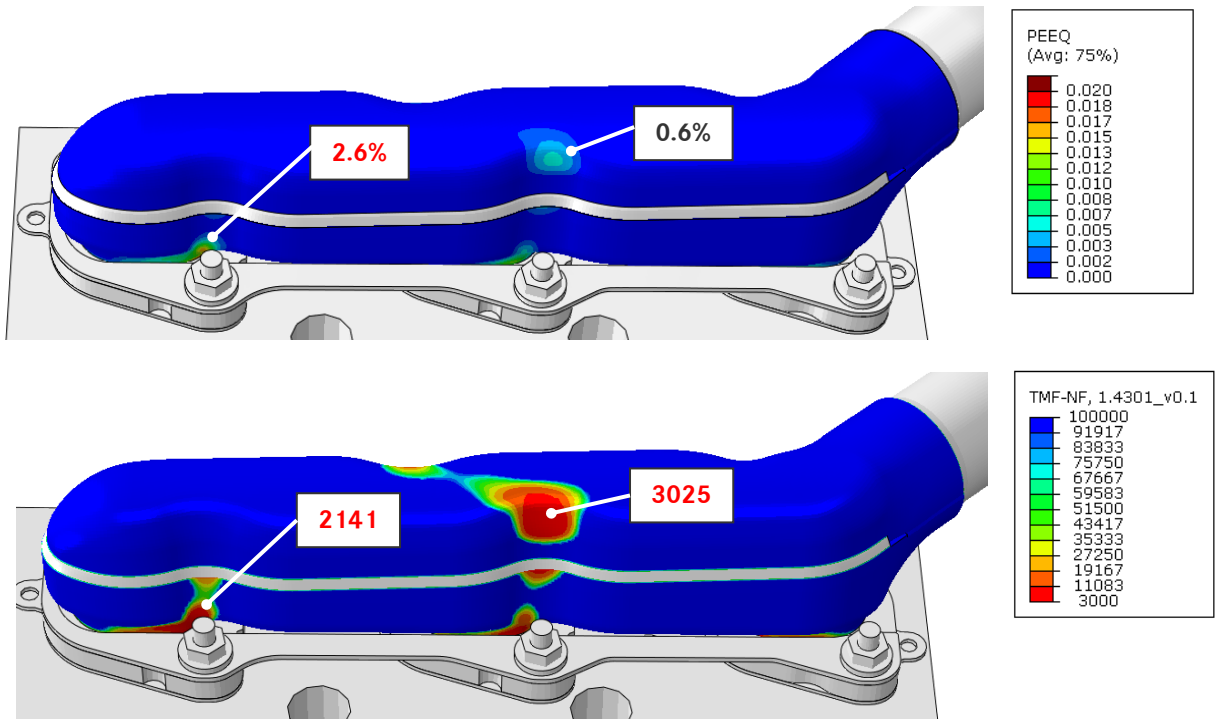

Fig. 9: Application example: Loading of outer shell.

6. CONSIDERATION OF SEAM WELDS.

As described in Section 1, LSI exhaust manifolds have some welds. For the calculation of the welds, the procedure to assess lifetime was extended. For this purpose, LCF experiments were carried out with welded test specimens. The aim of the LCF experiments was to evaluate the pure material behavior of the weld and not to consider the geometry. After adapting the material model and life model, the geometry can then be considered by a realistic modeling of the weld in the FE model.

Specimens for LCF-Tests

Specimens were made from two tubes which were circumferentially welded together, Fig. 10a. As described in Section 3, the tube shape was chosen to be able to pulse using both, tensile and compressive loads. In order to eliminate the influence of geometry, the specimens were machined and grinded from the outside and rubbed from the inside, so that the weld was no longer visible, afterwards. All samples were examined prior to processing with computed tomography, Fig. 10b, to exclude binding errors and inclusions and find if the cross-section of the seam was sufficient for mechanical processing. In addition, some samples were examined in microsection. Fig. 10c shows that the structure of the weld is very coarse and the transition to the base material is very abrupt, this means there is only a very small heat affected zone.

(a)

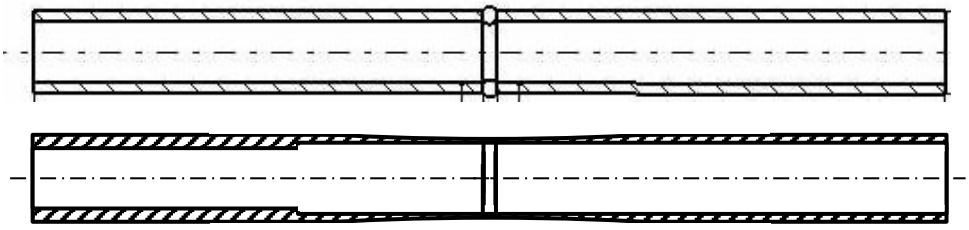

(b)

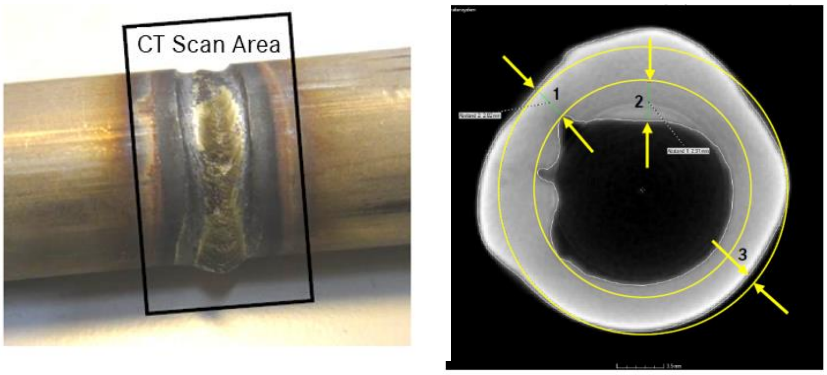

(c)

Fig. 10: (a) Welded specimen before and after machining, (b) CT section of a welded specimen before machining, (c) weld seam in microsection.

LCF-Tests

With the welded specimens, LCF experiments were carried out analogously to the base material tests, but to a lower extent. Depending on the temperature level, there were several expansion horizons. As in the LCF experiments with the base material, the crack occurred shortly after crack initiation. That means, in these experiments the lifetime until crack initiation is nearly the same as the total lifetime. The fracture starts on the processing structure inside the pipe in the middle of the weld seam, Fig. 11a.

Regarding the ratio of the number of load cycles until crack between the base material and the weld, the average factor was about 3. For small strains, the factor was rather higher (factor 5) and lower for high strains (factor 2). The temperature also has an influence on this factor: at low temperatures factor 4, at high temperatures factor 2.5.

These dependencies are also visible in the lifetime lines of the LCF experiments, Fig. 11b. The lines of the welded samples are steeper than those of the base material. This results in the larger factor for large strains (→ black arrows). In addition, it can be seen that the distance between the lines of base material and weld at high temperatures is lower than at low temperatures. This results in the smaller factor at high temperatures (→ gray arrows).

(a)

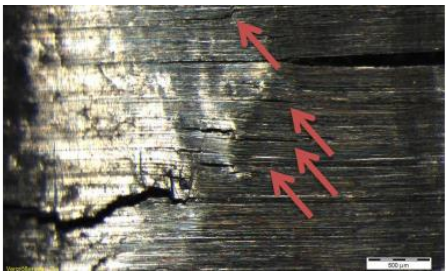

(b)

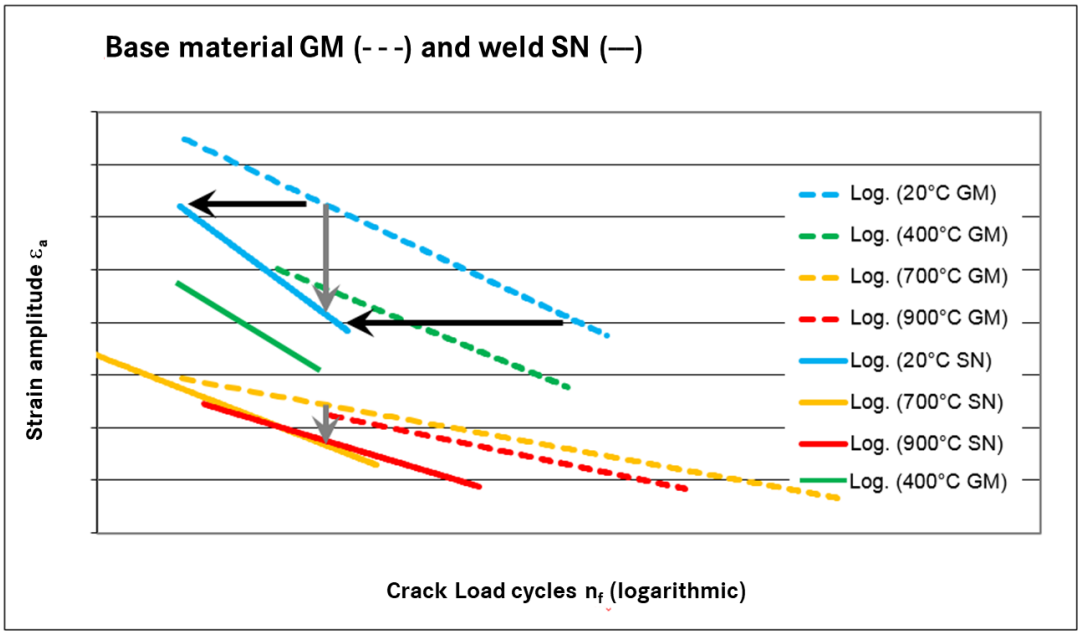

Fig. 11: (a) Fracture starts from the machining structure inside the pipe in the middle of the weld, (b) lifetime lines in comparison.

The experiments were evaluated with regard to their strain progressions. Some of the welded samples were provided with several measurement marks, Fig. 12a, to determine the strain in different areas around the welds (4-20 mm). This can be used to check how the expansion spreads over weld and base material. The weld itself is about 4mm wide. Fig. 12b shows the strain curves of an experiment at different measuring lengths. It can be seen that the extent of expansion is greater for smaller measuring lengths, ie in the weld seam area, than in the outer area. In addition, it can be seen that softening takes place in the weld area: The strains with small measurement lengths increase with the number of cycles. The elongation at 16 mm measuring length is constant, as this is the controlled variable of the test.

(a)

(b)

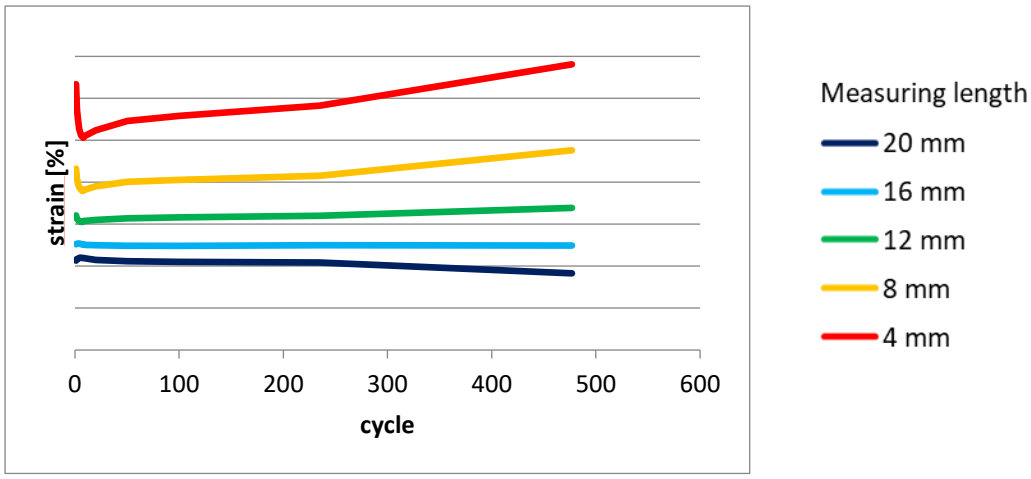

Fig. 12: (a) Sample with measuring marks to determine the strain in 5 areas, (b) course of strains at different measuring lengths.

In order to be able to assess the strain behavior even better, the strains of a test were split into their elastic and their plastic part, Fig. 13. This is possible using the data of the hysteresis curve.

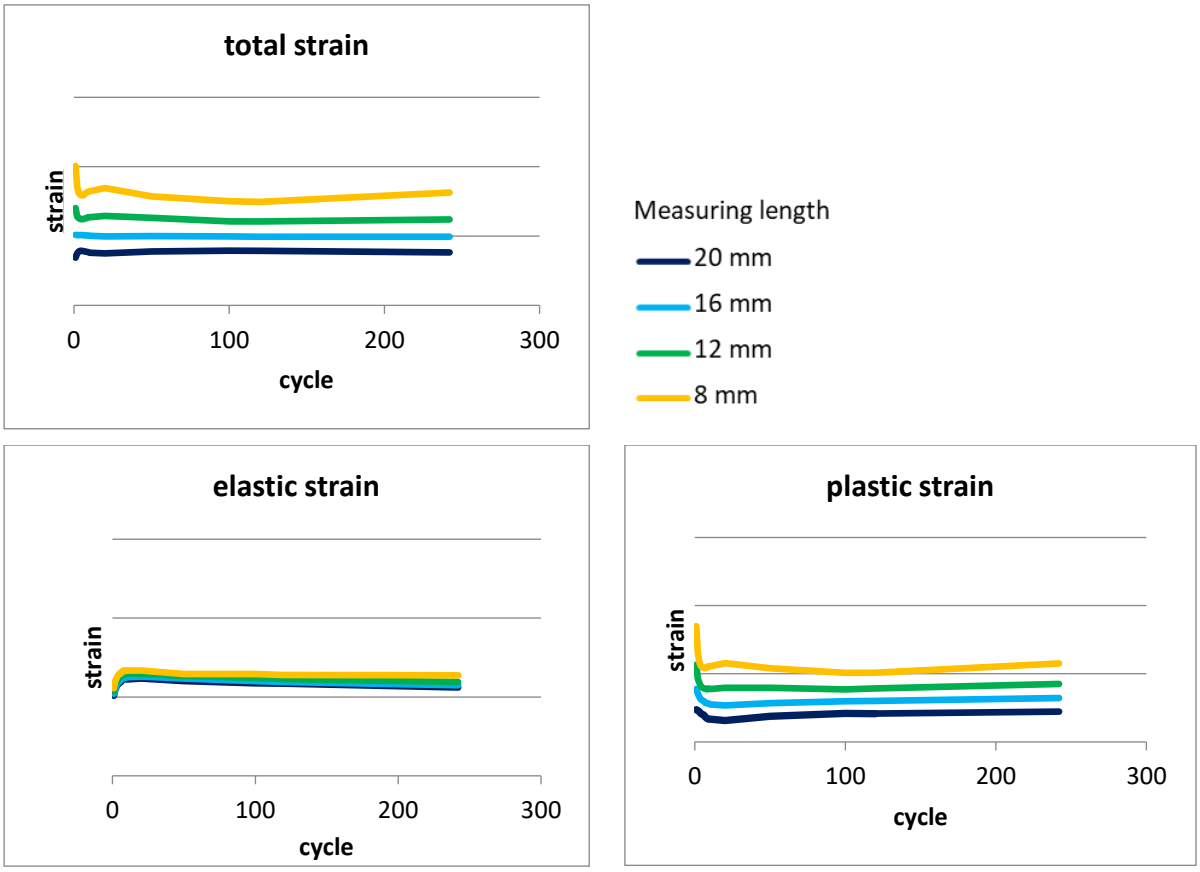

Fig. 13: Splitting of strain in elastic and plastic part.

The proportion of elastic strain is approximately equal in all strain areas and nearly constant. The plastic deformation is greater in the inner area than in the outer area. This suggests that the yield point in the weld area is lower than in the outer area. Therefore, in order to recalculate the LCF experiments, an FE model was created in which the yield strength was lowered compared to the base material. All other material properties were not changed. Fig. 14a shows an eighth model of the sample with lowered yield strength in the weld region. To represent the entire specimen, in the picture at the right, the model must be mirrored several times.

Using this model, all LCF experiments were recalculated. Fig. 14b shows some of the hysteresis curves resulting from this material model. The curves are in good agreement with those of the experiment. Therefore, the material model described can be used to model the welds of this material.

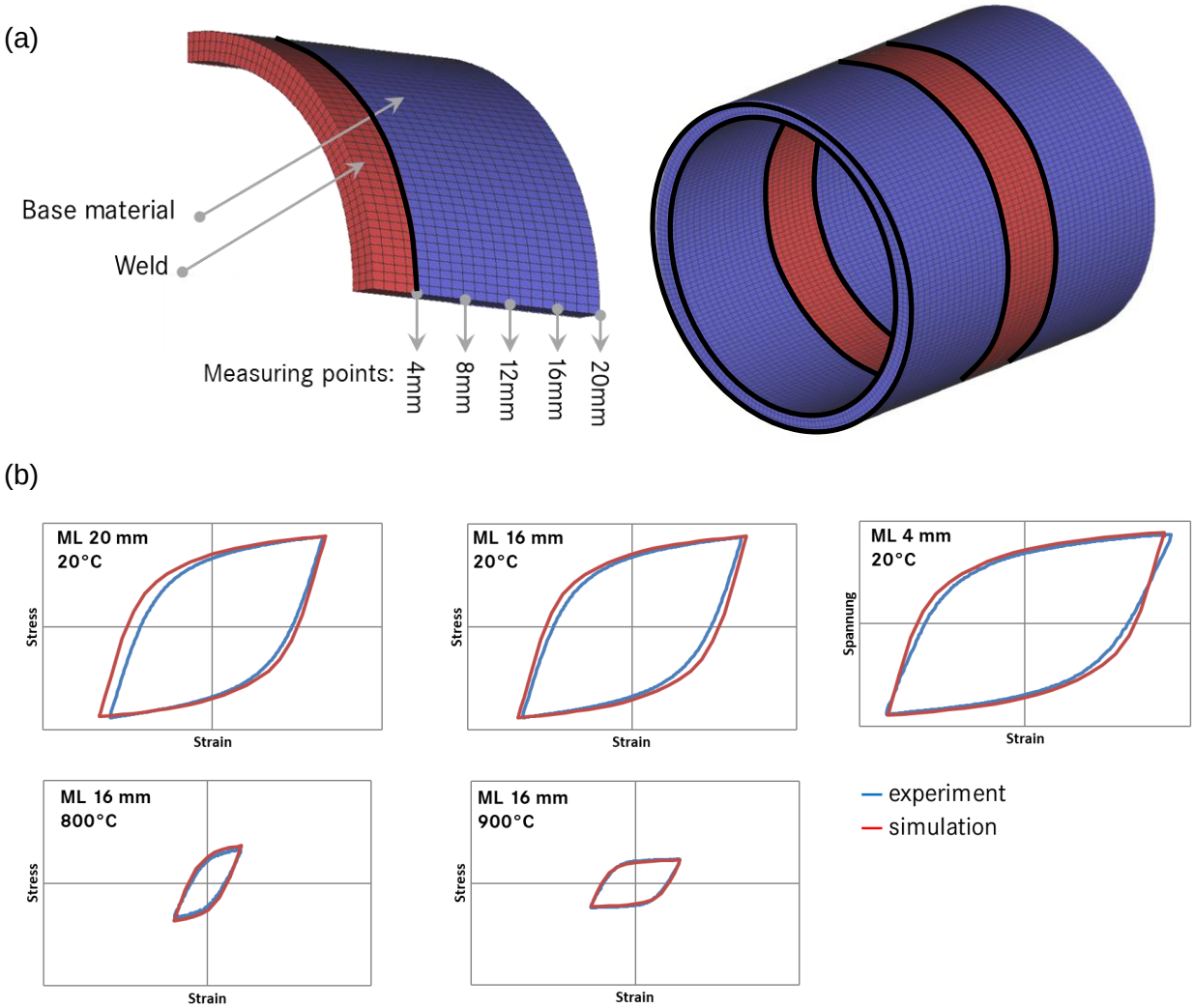

Fig. 14: (a) Model of eighth for a LCF specimen with weld, (b) comparison of hysteresis curves experiment / simulation as an example.

Afterwards, the lifetime model developed for the base material was applied to the FE results in order to find out whether reliable predictions can be made with the existing life model, or whether a new life model needs to be developed. Fig. 15 shows the correlation of the calculated lifetimes with the experiment. The predictions of the simulation, apart from a few exceptions, lie within the factor 2 band. This prediction accuracy was accepted as sufficient so that the procedure described can be used in practice.

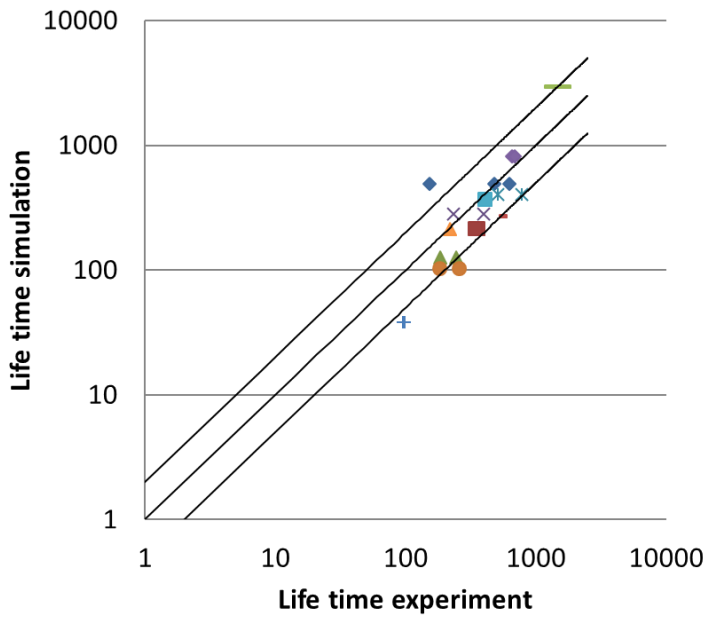

Fig. 15: Correlation between Simulation and experiment using the adapted material model for welded specimens.

7. OUTLOOK

The described material and life model was created for all essential base materials. However, the examination of the welds has only been carried out for one material combination. For the evaluation of other material combinations, it is necessary to carry out further investigations on welded LCF samples with the combinations of weld metal with base material(s) used in production.

In addition, further validation studies were planned. In order to be able to detect the crack initiation in the validation test even better, the validation test should be modified so that the crack on the outside of the test specimen starts. This requires a change in the geometry of the specimen.

Practical experiences are currently being collected with the illustrated material and service life models, and it is observed how good the applicability and predictive accuracy of real components are.

REFERENCES

[1] Wendt, M., Rehm, W.: Development of models for life estimation for LSI exhaust manifolds. Proceedings of the “Fourth International Conference on Material and Component Performance under Variable Amplitude Loading (VAL4)”, DVM Berlin, 2020

[2] Mayr, T.: Experimentelle und rechnerische Untersuchungen zur Lebensdauerbewertung thermomechanisch hoch beanspruchter Gussbauteile im Abgassystem von Nutzfahrzeugmotoren. Shaker-Verlag, Aachen 2011

[3] Effizienz im Blick. Technicity, 01/2012, pp. 16-17

Corresponding author: mareike.wendt@daimler.com